Applied Composite Materials
https://doi.org/10.1007/s10443-025-10343-3

RESEARCH

Damage Assessment of Polyamide-Based Woven Composites Using Multi-Directional Lamb Waves After Fatigue or Impact Loading

Nada Miqoi[1,2,3] · Pascal Pomarède[1] · Fodil Meraghni[1] · Nico Félicien Declercq[2] · Stéphane Delalande[4]

Received: 5 December 2024 / Accepted: 3 May 2025

Abstract
This study presents a novel experimental methodology designed to assess damage in woven glass fibers reinforced polyamide 6,6/6 composites, specifically subjected to low-velocity impact and cyclic tensile loading. Conventional ultrasonic testing techniques often fail to detect subtle material degradation, particularly when dealing with barely visible impact damage (BVID), which can go unnoticed but still significantly compromise structural integrity. In contrast, the proposed approach utilizes multi-directional ultrasonic Lamb wave analysis, a more advanced technique that offers greater sensitivity and precision in identifying damage at various stages of the composite's lifespan. In this work, a damage indicator is defined based on the velocity profile of Lamb waves, which are sensitive to changes in material properties such as stiffness degradation. The Lamb wave-based methodology is rigorously validated through detailed comparisons with X-ray tomography. These comparisons reveal strong correlations between the two techniques, highlighting the effectiveness of the proposed ultrasonic approach in detecting BVID. Moreover, the study demonstrates that this methodology is not only highly sensitive but also scalable, making it suitable for industrial applications where automated inspection of composite components is essential. The proposed method offers a significant advancement in non-destructive testing (NDT) techniques based on Lamb wave diagnostic tools in composite material testing.

Keywords Ultrasonic Lamb waves · X-ray tomography · Woven reinforced composite material · Low velocity impact tests · Fatigue tests · Damage investigation

1 Introduction

The demand for lightweight and durable materials has driven the adoption of polymer-based composites in industries such as automotive and aerospace [1, 2]. These materials offer significant weight reductions compared to metallic structures, contributing to energy

Extended author information available on the last page of the article

efficiency. However, their application introduces unique challenges, including complex damage mechanisms such as matrix cracking, fiber breakage, and delamination, which are difficult to detect and monitor during the early stages [3–6].

The damage mechanisms could be complicated to detect and monitor directly from standard imaging techniques, especially at their initiation and accumulation. More specifically, when used in the automotive industry, the composite parts must withstand impact and repetitive loading, such as fatigue loading, during their in-service life. Indeed, even a low-velocity impact can induce internal damage of a composite structure, decreasing hence its life span [7–9]. However, these events only let minor damage traces on the impacted surface, which might not be visible macroscopically but could induce cracks inside the material, thus remaining undetected in visual inspection. This type of damage is commonly called 'Barely Visible Impact Damage' (BVID). Several parameters are known to affect the criticality of the impact event and are detailed in [3, 10]. Furthermore, cyclic loading induces damage propagation and accumulation, which can result in disastrous in-service rupture. In addition, the probabilistic nature of the fatigue solicitation and the lack of detectable fatigue limit, especially for the plastic-based composite material, make its assessment critical. This is due to the complexity of the damage mechanisms [11, 12].

The fiber architecture and the direction of loading significantly influence the damage propagation and mechanical performance under fatigue loading, impacting crack initiation and growth [13]. It is essential to mention that the coupling of fatigue and low-velocity impact loading will lower the performances and, consequently, the life span of composite parts even further. It is worth noticing that this coupling will not be discussed in the present study, which focuses, as a first step, on uncoupled loading configurations,

In order to avoid catastrophic failure, it is critical to control the integrity of composite structures with efficient Non-Destructive Testing (NDT) techniques that could detect the damage at its earliest stage. Several methods have already been investigated in the literature such as infrared thermography [14, 15], X-ray tomography [16–18] and ultrasound. Infrared thermography can be easily applied but is less effective than ultrasonic techniques in imaging minor defects, especially in depth [19, 20]. High resolution can be achieved with X-ray tomography, but it is an inspection approach that can be long and is ionizing thus presenting health risks to human operators. In addition, a great advantage of using ultrasound is its versatility. Ultrasound can be applied at oblique incidence to better describe the defect [21]. Sound propagation velocities can be used to reconstruct a full stiffness tensor and monitor its evolution with an applied loading [22–24]. When used in the non-linear regime, ultrasonic-based methods could also be more effective for damage detection [25, 26]. These two techniques could provide operative damage indicators [24, 27]. More specifically, Katunin et al. [28] also identified ultrasound, infrared thermography and X-ray Computed Tomography as the main methods for BVID evaluation after reading documents issued by US et EU aviation Safety agency. Ultrasound has also been found to be the most reliable and portable solution in [29]. Finally, the damage in impacted composite samples can be characterized by ultrasound using the Permanent Indentation and stiffness components measurements [30].

However, one major issue when using particular ultrasonic-based techniques is the scan duration [19, 20]. For inspecting extended structures, it is more suitable to use ultrasonic Guided Lamb Waves (GLWs) [31–33], as it allows a faster inspection of the structure. The use of GLWs for damage inspection of composite material is extensively discussed in the literature and has proved its effectiveness [34–37]. However, the propagation of GLWs in

composite plates is complex due to different parameters such as dispersion, multi-mode characteristics, and direction dependency of the wave velocity [38]. Most of the GLWs methods described in the literature involve localization of the impact area using reconstruction algorithms. For these methods, the signals acquired on the current sample are usually compared with a reference signal (baseline) [32, 39–42]. However, these methods need several measurements, performed at different location of the sample to be effective. These methods are more Structural Health Monitoring (SHM) methods rather than inspection methods that can be used "on the fly". A method involving less sensors and measurement for the damage detection of sample on-site is therefore more appropriate.

This paper aims to describe a GLWs-based method to detect and quantify damage in samples impacted at low energy levels or subjected to cyclic tensile loading. The method is based on Time of Flight (ToF) measurement in different propagation directions. The ultrasonic (US) ToF is a function of the material stiffness properties. A damage indicator, defined from these measurements, is proposed. Several levels of damage are generated in the materials using two loading methods: impact and interrupted fatigue loadings. Comparison with results from X-ray micro-tomography analysis is carried out for the two loading configurations to validate the proposed damage indicator as a reliable assessment. This work investigates a polyamide 6,6/6-based composite reinforced by three layers of woven glass fibers. The material and the experimental setup for the impact and fatigue tests are first discussed. The GLW method is then described. Finally, the results are presented and discussed on samples subjected to impact at different energy levels or fatigue loading at different stress amplitudes and cycle numbers, as well as the comparison with the X-ray tomography analysis.

2 Material and Experimental Procedures to Induce Damage

This study has been conducted on a balanced polyamide 6,6/6 reinforced with three layers of 2/2 twill woven glass fibers, oriented 0°/90°. The composite material has been produced by thermo-compression molding process, in the shape of plate with a total thickness of 1.53 mm. The tested samples have been previously conditioned at a relative humidity level of 50% (RH50). The microstructure and the architecture of the material reinforcement are presented in Fig. 1.

The mechanical characteristics of the studied composite are summarized in Table 1. More details about the composite are given in [30].

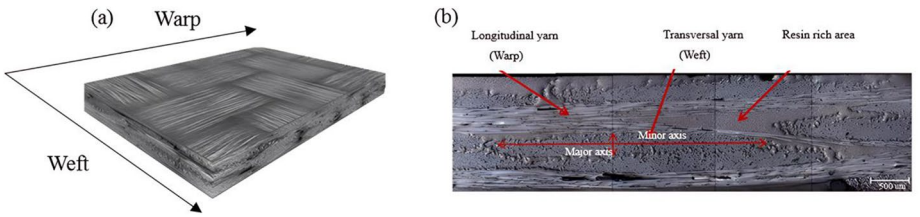

Fig. 1 Mesostructure (**a**) and microstructure microscopic observation (**b**) of the woven glass fabric-PA66-6 composite showing warp (0°) and weft orientation (90°) (Inspired from [24])

Table 1 Mechanical characteristics of the studied PA 66/6 reinforced with woven glass fibers composite at 50% of relative humidity (RH50) and at room temperature

Mechanical characteristics	Density	Fiber volume content	Young modulus warp direction (0°)	Young modulus weft direction (90°)	σ_{UTS} warp direction (0°)	ϵ_{UTS} warp direction (0°)
Values	1.78 g/cm^3	43%	17.7 GPa	18.1 GPa	303 MPa	1.9%

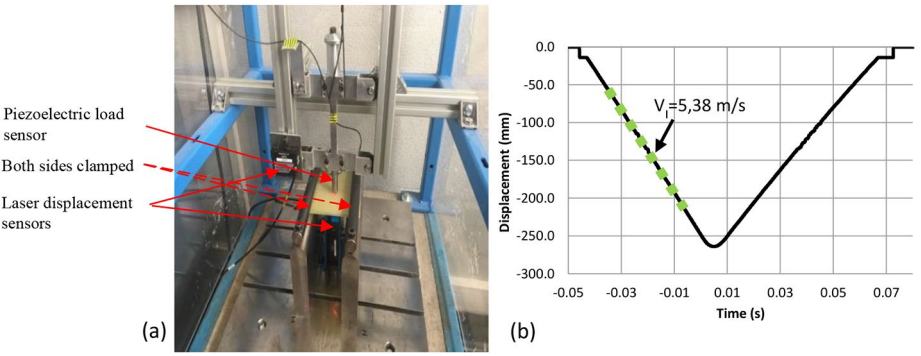

Fig. 2 (**a**) The experimental device used to perform drop-weight impact tests shows a piezoelectric load sensor, a first laser displacement sensor that monitors the striker's displacement, and a second one placed under the clamped sample to record the deflection. (**b**) Example of impactor displacement/time curve. The measured displacement is used to compute the real impact energy

2.1 Drop Weight Impact Experimental Setup

Eight samples of rectangular shape 100×150 mm^2 are cut from the manufactured plate using a water-cooled circular saw. This shape is chosen in agreement with the ASTM D7136/D7136M standards. To ensure any cutting process-induced initial damage, the cut samples, and particularly their edges, have been priorly investigated using ultrasonic C-scan imaging.

The cut samples have been subjected to impact tests at 7 impact energy levels. The impact tests are performed using a drop-tower equipped with a 1.02 kg striker that has a hemispherical end with a diameter of 16 mm. The plates are clamped at both ends, as illustrated in Fig. 2.a, and their displacement is measured using a laser displacement sensor (Example of a measured curve can be seen in Fig. 3.b). A piezoelectric load sensor and another laser sensor measure the force and displacement of the striker during the impact tests (Examples of measured curves can be seen, respectively, in Fig. 3.a and Fig. 2.b). The objective is to remain within the BVID regime and examine various stages of induced damage in the sample, as demonstrated later in this work. This will validate the reliability of the proposed NDT method for early damage detection. To this end, the seven impact energy levels are carefully chosen by varying the height of the impact. The samples selected for the rest of the study and their real impact energies, indicated in the Table 2, are calculated using force/displacement acquired with the experimental set-up sensors. The 0 s, on the time axis of all the mentioned graphs, corresponds to the time of contact between the sample and the impactor. From Fig. 3, the increase of the force applied on the sample and its displacement

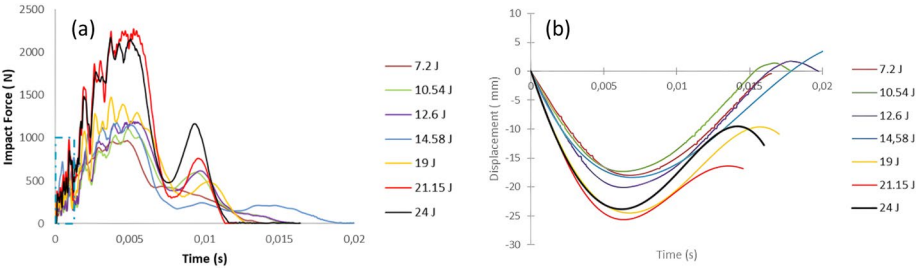

Fig. 3 (**a**) Force-Time curves and (**b**) the samples' displacement function of time for the seven chosen samples. The increase of both quantities is clearly visible when increasing the impact energy. A higher energy regime is also noticed for the samples impacted at 19 J, 21.15 J and 24 J

Table 2 The experimental set-up sensors obtained the real impact energies considered in this study. They are chosen to remain in the BVID regime. One sample is kept in its pristine state for comparison

Impact energy (J)	0	7.2	10.5	12.6	14.6	19	21.1	24

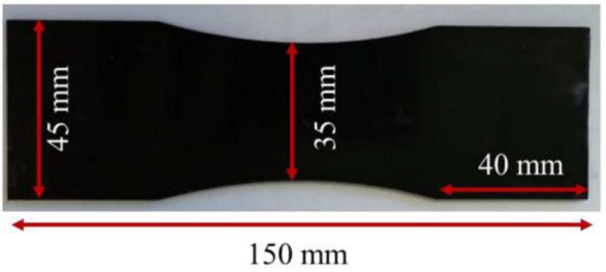

Fig. 4 Dimensions of the dog bone-shaped samples used for the fatigue tests

when increasing the impact energy is clearly visible. The appearance of a higher energy regime for the samples impacted at 19 J, 21.15 J and 24 J is also noticed.

2.2 Fatigue Experimental Setup

For the fatigue tests, nine dog bone-shaped samples are machined using water jet cutting. The geometry shown in Fig. 4 is chosen to localize the load-induced damage in the center of the sample. The load-controlled fatigue tests are performed, at a frequency loading of 3 Hz, using a hydraulic uniaxial test machine, an MTS Hydraulic wedge grip. Three loading levels are considered: 35%, 45%, and 60% of σ_{UTS}, and, for each level, three percentages of the number of cycles to failure (Nf) are reached, namely: 50%, 60%, and 70% of Nf. The loading levels are chosen in order to remain in the central part of the Wöhler curve (Stress Vs Number of cycles) of the studied material. In Malpot et al. [43] this central part has been found to be located between 10^2 and 10^6 number of cycles to failure for a nearly identical material. This central part corresponds to neither the short-term strength or the endurance fatigue limit and is more of interest for the present study. The percentages of the number of cycles to failure (Nf) have been determined to be sufficient to generate some damage in the material studied.

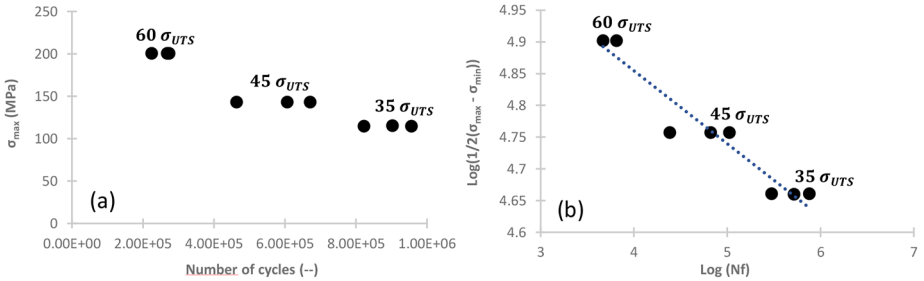

Fig. 5 Results from the preliminary fatigue study to determine the number of cycles to failure for 3 stress levels (**a**) Stress level function of the number of cycles to failure (**b**) Whöler curve in a logarithmic scale with a linear representation made with the Basquin model. The obtained number of cycles to failure is used for the interrupted fatigue tests inducing damage

Table 3 The nine combinations of parameters of the interrupted fatigue tests made to generate damage in the samples. The indicated number of cycles to failure were obtained from the basquin model

Loading level	35% σ_{UTS}			45% σ_{UTS}			60% σ_{UTS}		
Number of cycles to failure (Nf)	444 122			66 030			3 702		
Proportion of number of cycles to failure (%)	50%	60%	70%	50%	60%	70%	50%	60%	70%
Number of cycles	222 061	266 473	310 885	33 015	39 618	46 221	1 851	2 222	2 592

The number of cycles to failure for each loading level is previously determined from a fatigue-to-failure experimental campaign. Measurements points are obtained from this fatigue-to-failure experimental campaign and plotted on a Wöhler curve depicted in Fig. 5. From this figure, a significant dispersion of the number of cycles to failure is observed. This is expected for a composite material, especially for long lifetime. It will need to be considered in the later analysis of the induced damage evaluation using the proposed NDT method.

The average number of cycles to failure, that is used for the interrupted fatigue tests, is determine using the Basquin model [44]. This model is only able to describe the central part of a Wöhler curve, which is appropriate for the loading level used in this study. The latter is expressed by:

$$\log(N) = \log(C) - m * \log(\sigma)$$

In this equation, N is the number of cycles, σ the stress load (half of the loading amplitude) and the C and m parameters of are determined by linear regression using the measurements points in a log/log diagram. The obtained Basquin curve is added in Fig. 5, and the nine selected parameters of the interrupted fatigue tests are indicated in Table 3.

3 Guided Lamb Waves Experimental Setup

The objective of this setup is to take into account the anisotropy of the material and use it in the design of the damage indicator. For this purpose, the velocity of the ultrasonic wave needs to be measured in different propagation directions. This provides a way to esti-

mate the residual stiffness properties of the investigated structures. Finally, GLWs provide an investigation operando tool that can be achieved easily on-site/in-service. Indeed, the technique only requires access to one side of the structure during damage inspection. The complication arises from the simultaneous propagation of multiple GLW modes at different velocities. As we are using a method based on velocities measurements, it is necessary to verify that the propagating signal is mono-modal and remains in a non-dispersive regime, to simplify the experimental procedure when using the GLWs. In order to do so, we should ensure that the frequency of the propagating mode is low enough. The dispersion curves, for wave propagation along 0°, of the studied material are calculated using the "Disperse" software, developed at the Imperial College NDT lab (Fig. 6). The computation process requires the thickness and the stiffness tensor of the material. The latter is estimated by periodic homogenization computation [45–47]. From the simulated curves showed in Fig. 6, one can notice that only the A0 and S0 modes can theoretically propagate for a frequency from 0 kHz to 250 kHz.

Two V103-RM Olympus contact transducers, with a center frequency of 1 MHz, are employed in transmission mode. A single 150 kHz sinusoidal pulse, with a 10 V peak-to-peak amplitude, is generated through a waveform generator, a Hewlett Packard 33,120. This emitting signal is chosen, to avoid overlapping signal effect that could appear we the pulse duration is too long. A Krohen-Hite model 7500 amplifier is used a significant a significant decrease of the signal is expected in the composite samples. The chosen transducers have a large bandwidth and can be used effectively at this frequency, as verified after comparison of the received signals amplitude at different frequencies.

A transducer holder is manufactured using 3D printing to keep the distance between the transducers to 6 cm (Fig. 7.b). This distance was selected to avoid any overlapping mode while keeping a high signal to noise ratio. In addition, a sample holder (Fig. 7.a) is made by 3D printing, allowing 5° step rotations of the sample. Measurement is conducted in the range of α= [-30°; 30°] with a 5° increment to account for material anisotropy and ensure

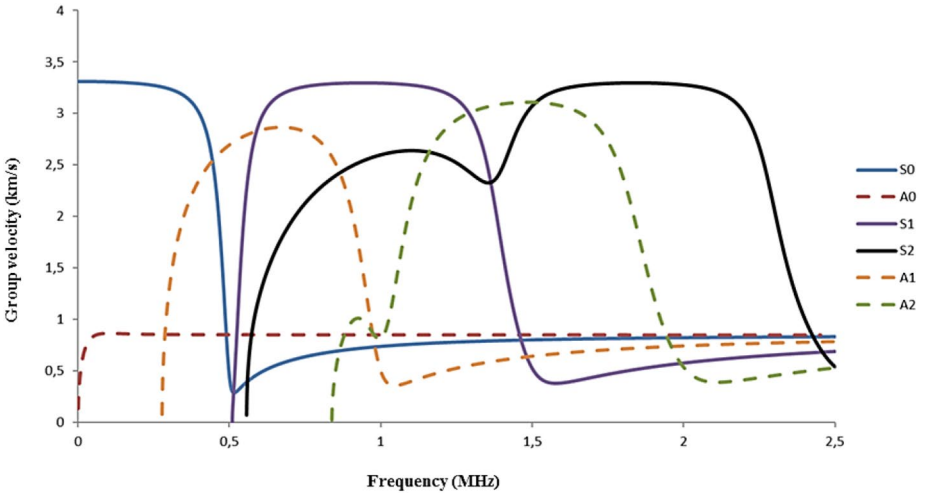

Fig. 6 Dispersion curves corresponding to the propagation of guided waves at 0° in the studied material showing the group velocity function of the frequency. They are calculated using the 'Disperse' software from the Imperial College NDT lab [24]

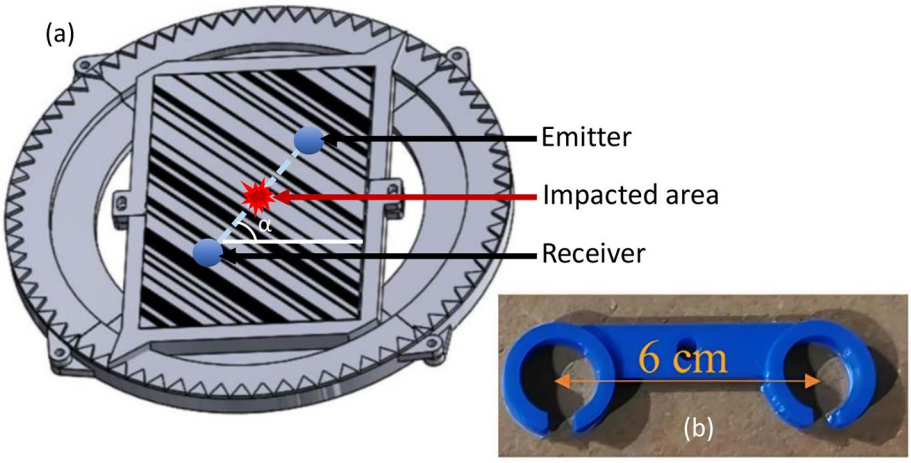

Fig. 7 Guided Lamb Waves experimental set-up. An ultrasonic emitter and receiver are put with the impacted area in between. The direction of the wave's propagation is given by the angle α. The system in (**a**) allow the rotation of the sample to be consistent and the system in (**b**) allow the distance between the transducers to remain 6 cm

comprehensive directional analysis of wave propagation. Measurements are not extended for higher angles due to limited sample size, especially for fatigue-fatigue loading. A schematic representation of the experimental set-up is given in Fig. 7. A 5-axis robotic scanner is used to hold this system and maintain the same pressure with the inspected composite material and avoid any coupling issues.

For each acquired signal, the Time of Flight (ToF) is determined by cross-correlation by convoluted the acquired signals with a reference signal. As the input pulse and the propagated guided wave signal differ in shape significantly, due to the dispersion effect, it was chosen to use an acquired one as a reference. It is measured on a reference, undamaged sample, for a 0° propagation direction (along the fiber direction). The signal used as a reference is indicated in red in Fig. 8.a. An example of acquired signal and calculated correlation signal is also indicated in Fig. 8.b with the obtained ToF circled in green. Based on these measurements, it has been assessed that the velocity of the first wave packet corresponds to the one of the S0 mode. It has been decided to dedicate the rest of the study on this mode analysis. Indeed, as showed in [48, 49], the S0 mode is more sensitive to the detection of internal damage, whereas the A0 mode is more sensitive to surface damage. This is due to the nature of their displacement fields, with the S0 mode being a quasi-axial mode and the A0 mode being a quasi-flexural mode. Since our proposed NDT aims to quantify the damage generated inside the composite material after impact or fatigue, the S0 mode is more appropriate.

The obtained dispersion curves are then used to predict the evolution of the S0 group velocity when varying the propagation direction on the investigated material. For this purpose, the S0 dispersion curves are computed for different propagation angles, from −30° to 30°, with 0° being the warp reinforcement orientation. An approximation curve is calculated to provide a clear trend of the velocity profile evolution. The best fit is achieved

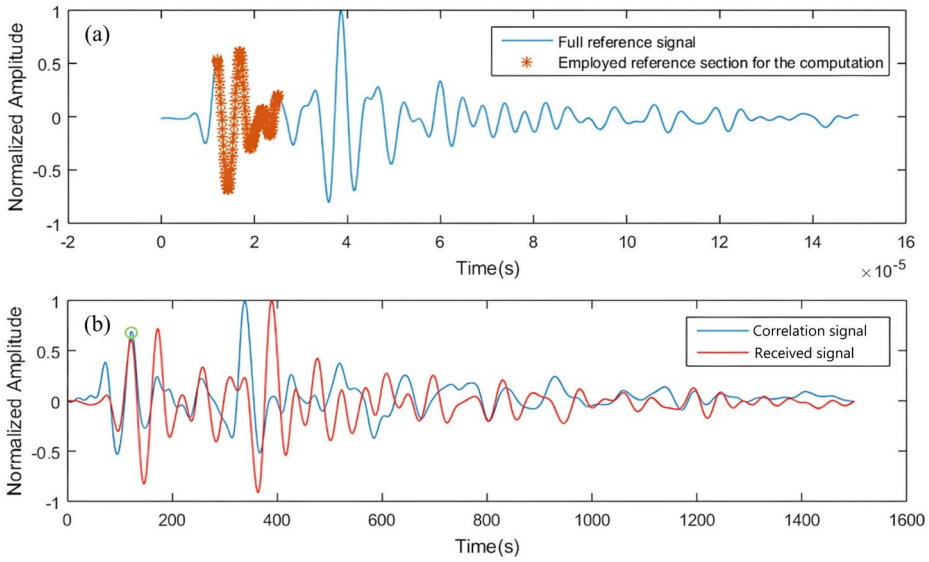

Fig. 8 (**a**): Reference signal used for the cross-correlation. (**b**) Received signal (in red) and correlation signal (in blue) with the indicated Time of Flight determined by cross-correlation (circle in green)

with a fourth-order polynomial approximation. The obtained group velocity profile and the approximation curve are then normalized and depicted in Fig. 9.

A new damage indicator, D, is proposed to monitor the damage evolution with respect to the impact energy level. It is estimated as the ratio of the area under the group velocity profile, measured on a sample impacted at a given energy level, $A_{damaged}$, and the area corresponding to the non-damaged state, A_{ref}. This is illustrated, on Fig. 9, with the two group velocities curves, for a damaged and undamaged cases. They have been calculated for the 0° propagation direction, which corresponds to the warp fibers' direction. The curve for the damaged case is obtained from simulated data, from "Disperse", for a sample whose stiffness properties have been decreased. Therefore, the damage indicator (D) is expressed as follows:

$$D = 1 - \frac{\mathrm{A_{damaged}}}{\mathrm{A_{ref}}}$$

In this equation, $A_{damaged}$, the surface under the approximation curve of a damaged sample, and A_{ref}, the one under the approximation curve of the reference sample.

4 Drop-Weight Impact Test: Damage Analysis Specimen Impacted at Different Energy Levels

The proposed experimental setup is used for all seven impacted samples and the non-damaged sample. For the sake of clarity, only some velocity profiles are illustrated, in Fig. 10, for low, moderate and high impact energy levels. The interpolation curves are also plotted

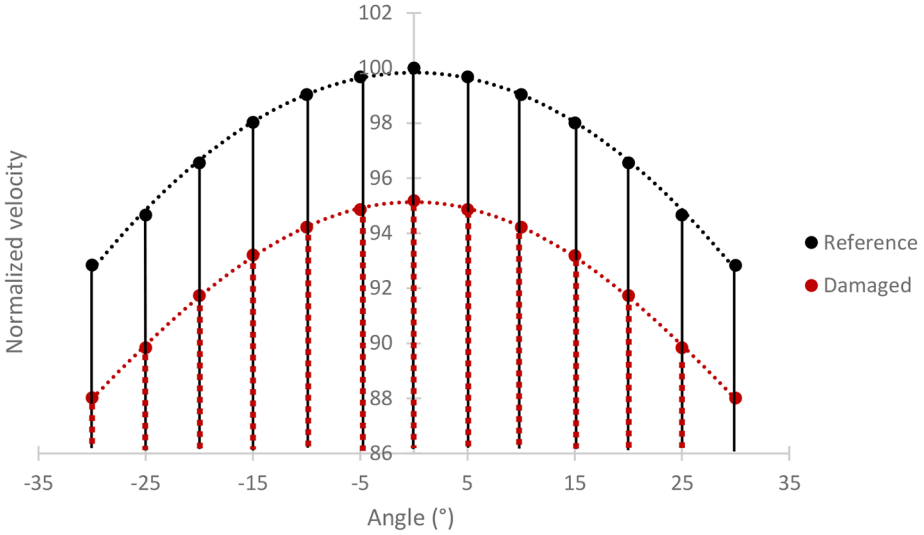

Fig. 9 Simulated normalized group velocity profile of the studied material, obtained using the 'Disperse' software from the Imperial College NDT lab, as a function of the propagation direction angle. 0° is set as the warp fibers' direction. Profiles for typical reference and damaged samples are given. The fourth-order polynomial approximation curve is also depicted

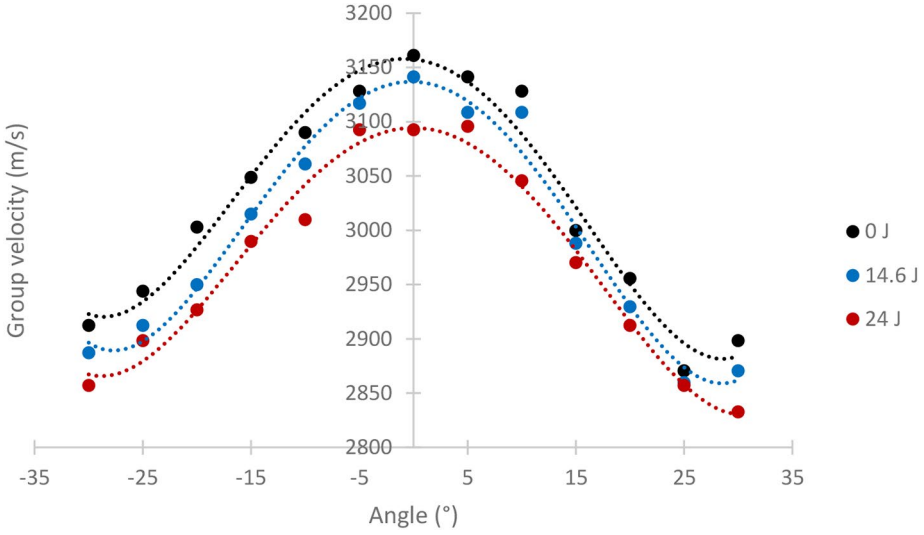

Fig. 10 Measured group velocity profiles for different selected impact energies for propagation velocities from −30° to 30°. Measure on non-impacted samples and samples impacted at measured energy of 14.6 J and 24 J are depicted. A fourth-degree polynomial curve approximation is also shown for each selected impact energy with an R^2 of respectively 97%, 98% and 98%

to highlighted the velocity evolution trends with respected to propagation direction. One can observe that the velocity profiles of the impacted samples differ from the ones measured on the reference sample. Indeed, the overall measured velocities decrease when compared with those measured on non-damaged sample. In addition, this gap increases with the impact energy. This can be explained by the decrease of the stiffness properties at the early stage of damage initiation and its accumulation when the impact energy increases. The values of the damage indicator D are then calculated for all eight samples and plotted in Fig. 11 as a function of the impact energy. A clear and consistent increase in the damage indicator D with rising impact energy is observed. Three different regimes can be distinguished. First, the value of the damage indicator remains low and starts increasing when reaching 10.5 J, then a stabilization regime occurs from 10.5 J to 14.6 J, where the damage indicator remains at a value of 0.0025. Finally, the value of D significantly increases for the three samples impacted at energies from 19 J to 24 J. One can observed that the damage indicator reaches a value of 1.2% when the damage energy increases from 21.1 J to 24 J.

In order to assess the results obtained using GLWs experiments and the levels reached by the damage indicator, an investigation of the damage induced by the impact loading is made using X-ray tomography. All the samples are analyzed at a resolution corresponding to a voxel size of 12 µm. The EasyTom (Nano) device, developed by RX Solutions, is used to handle the 2D images. The latter are then post-processed using the X-act software for the 3D reconstruction. The obtained images show that:

- No observable damage is generated for the 7.2 J impact.
- The first signs of damage emerge in the non-impacted surface for the 10.54 J impact (Fig. 12.a). This initial damage is characterized by matrix cracks confined to the sample's first layer. As the impact energy increases, from 12.6 J to 14.6 J, the damage in the

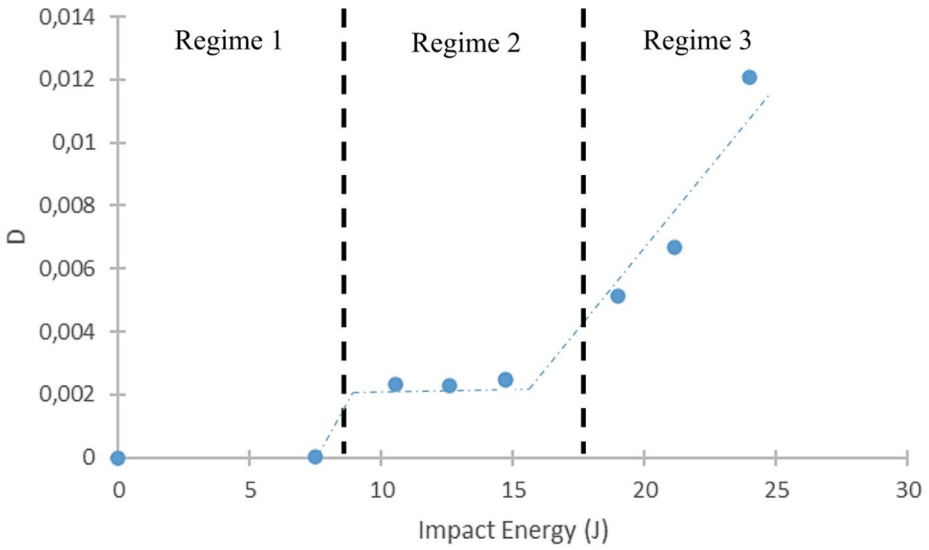

Fig. 11 Evolution of the proposed damage indicator, D, with increased impact energy. Three regimes are distinguished. First, no increase of D before 10.5 J is noted, and then it increases and stabilizes until 14.6 J. Finally, it increases significantly until 24 J

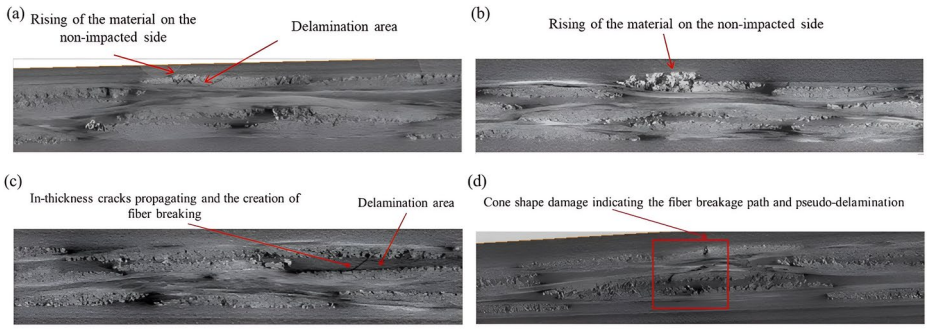

Fig. 12 X-ray tomography imaging of some impacted samples; a: 10.5 J, b: 14.6 J, c: 19 J, and d: 24 J. We can see the criticality of damage increasing with the impact energy. Different damage mechanisms such as matrix cracks, delamination, and fiber breakage are generated and propagate from the first layer (**a**, **b**) to the 2nd (**c**) and finally, the 3rd and last layer of the sample (**d**)

first layer escalates, as depicted in Fig. 12.b.

- Then, when reaching 19 J and 21.1 J, one observes the matrix cracks' growth until the sample's second layer, as seen in Fig. 12.c.
- Finally, from Fig. 12.d, the matrix cracks reach the 3rd and last layer of the material for the 24 J impact.

The X-ray tomography qualitative analysis of the damage accumulation with the impact energy aligns with the proposed damage indicator regimes. The same regimes are evident in the obtained values of the damage indicator, thereby confirming its relevance when used for impacted samples.

5 Damage Analysis on Specimens Subjected to Tension-Tension Fatigue Loading

This section investigates damage evolution and accumulation on specimens subjected to stress-controlled fatigue loading at different conditions. As mentioned in Table 3, three stress levels have been applied: 35%, 45% and 60% of the ultimate strength (σ_{UTS}). Each fatigue test configuration has been interrupted at three levels of cycle to failure: 50%, 60% and 70%. This results in nine different fatigue loading configurations. Similar to the previous section, the samples are investigated using the proposed GLWs-based method and the values of the damaged indicator D are estimated. The latter are exhibit in Fig. 13, with the percentage of the levels of cycle to failure as the x axis for an easier comparison between the loading configurations. From this figure, it can be noted that the values of the damage indicator, D, always exhibit a significant difference when compared with the undamaged sample (D = 0). This means that the GLWs-based investigation technique can discriminate the damage state from the pristine one of the investigated samples. As characteristic of fatigue loading, the damage exhibits a more diffuse state with less localization compared to the concentrated damage seen in impacted specimens, due to the gradual accumulation of micro-cracks over multiple cycles. Accordingly, more scattering is observed on these measured values of the damage indicator, as shown in Fig. 13. This makes the correlation

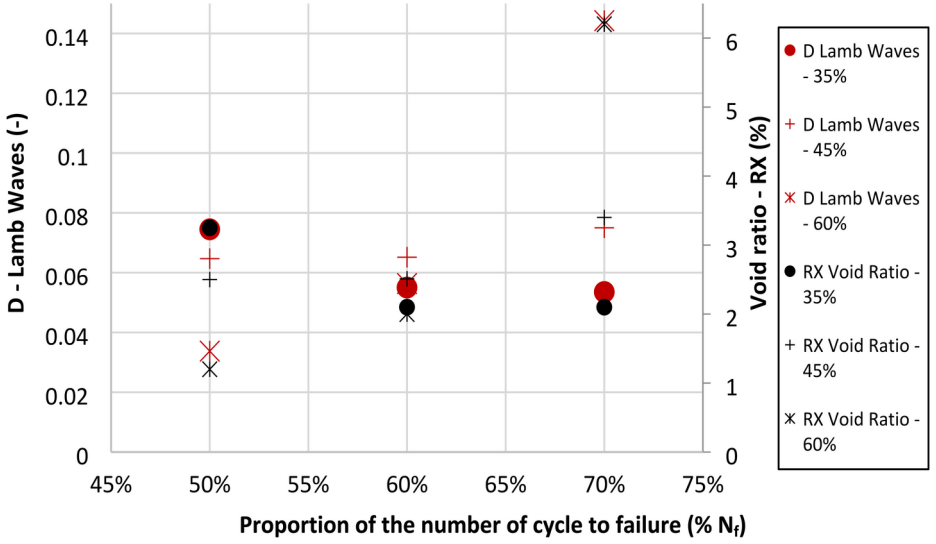

Fig. 13 Comparison between the proposed damage indicator D (in red) and the void volume ratio measured from X-ray tomography imaging (in black). Damage is generated from fatigue loading at a: 35% $\boldsymbol{\sigma}_{\boldsymbol{UTS}}$, 45% $\boldsymbol{\sigma}_{\boldsymbol{UTS}}$, 60% $\boldsymbol{\sigma}_{\boldsymbol{UTS}}$. Three percentages of the number of cycles to failure (Nf) are used for each aforementioned percent of $\boldsymbol{\sigma}_{\boldsymbol{UTS}}$. An excellent agreement between the two indicators is observed despite the high dispersion in the results. It is worth mentioning that the decrease of the void ratio and of D for 35% $\boldsymbol{\sigma}_{\boldsymbol{UTS}}$ is due to the variability of the fatigue behavior and the use of different sample for each loading configuration

between the loading and the damage evolution difficult, notably for the low applied stress (35% of σ_{UTS}). The next step involves assessing the proposed GLWs-based method to demonstrate its ability to quantify the induced damage accurately.

To this end, it is proposed to examine the samples utilizing X-ray tomography. As shown in Fig. 14, the three main damage mechanisms observed are: transverse yarn cracks, longitudinal cracks, and pseudo-delamination. One can notice, for instance, that the longitudinal and transverse yarn damage evolve from one layer to another when the number of cycles increases from 50 to 70% for the sample loaded at 35% of σ_{UTS}.

As mentioned earlier in this article, the measured damage is exhibiting scattering results, one must enrich these results by a direct quantitative evaluation using X-ray micro-tomography. The measurement of the void volume ratio evolution appears to be an accurate estimation of the actual damage state of a material [24, 50, 51]. The quantitative assessment is performed by careful grayscale thresholding, using the Avizo software, to discriminate visually the matrix and fibers from the cracks. The matrix and fibers of the composite exhibit distinct X-ray absorption values, allowing them to be easily differentiated on a grey level map. Since air does not significantly absorb X-rays, voids within the composite samples are not easily visible. However, during 3D image reconstruction, voids appear as completely black volumes. To reduce noise in the images, median filtering was first applied to the raw results, followed by a despeckle filter to eliminate most of the remaining interference noise. The reconstructions were then segmented into three classes (void, matrix, and fibers) using grayscale thresholding. The Avizo software segmentation enables accurate estimation of the volume fraction for each of the three phases.

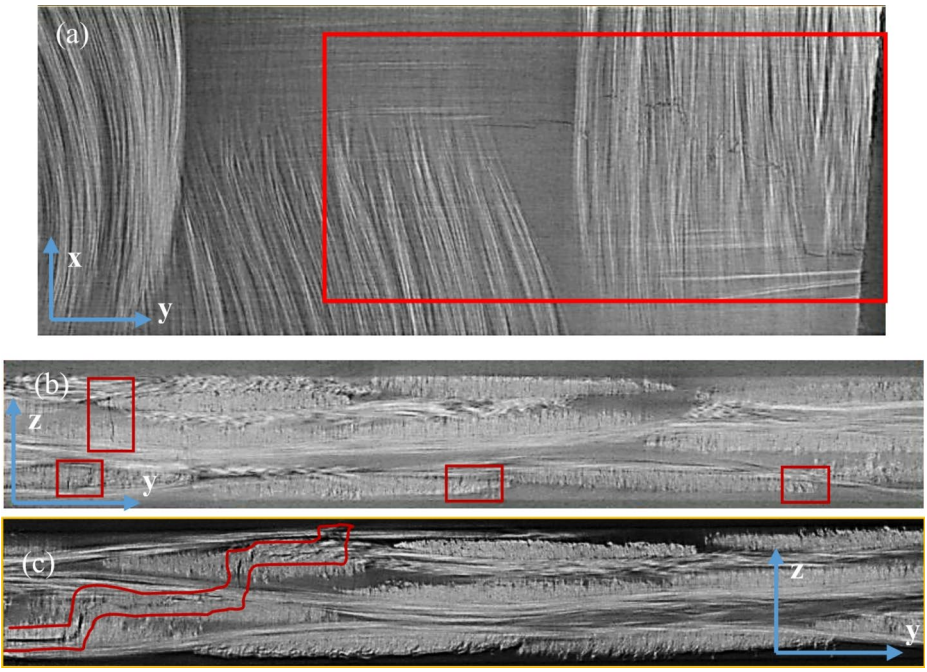

Fig. 14 Microcracks in the longitudinal and transversal yarn propagating in (**a**) the main plane and (**b**) from one layer to another of the sample loaded at 35% σ_{UTS} and 50% of the number to cycles. (**c**) Pseudo-delamination (highlighted in yellow) in the three layers of the sample loaded at 35% σ_{UTS} and 70% of the number to cycles

The acquisition is done at the center of the sample in order to compare with the same region investigated by the GLWs-based technique. The obtained results are reported in Fig. 13. It is critical to mention that not enough samples were used in the fatigue analysis to compare the evolution of damage from one sample to the other and draw conclusion of the fatigue behavior of the composite material. Indeed, the variability in a composite micro-structure is known to induce an important gap in the fatigue response. So only the variation of the two indicators value could be compared with each other to see if the proposed damage indicator D can be correlated with the void volume ratio induced by the impact.

As shown in Fig. 13, the damage indicator D, derived from the GLWs-based technique, aligns closely with the void volume ratio evolution measured via X-ray micro-tomography, with trends consistently matching across loading conditions. Indeed, even the unexpected decrease in the volume void ratio, for the fatigue loading of 35% $\boldsymbol{\sigma}_{\boldsymbol{UTS}}$(represented by circle markers in Fig. 13), is also detected by the damage indicator. This shows that the indicator directly reflects the actual damage state of the structure and that it may be even more reliable than the comparison presented for the impacted samples.

6 Conclusion

This study presents an experimental method for quantitatively assessing damage in polyamide 6,6/6-based composites reinforced with woven glass fibers. The proposed approach utilizes guided Lamb wave (GLW) analysis to define a damage indicator based on the velocity profile of ultrasonic wave propagation in multiple directions. This study addresses critical challenges in damage detection for lightweight composite materials used in the automotive and aerospace industries by focusing on low-velocity impacts and cyclic tensile loading scenarios.

The findings demonstrate the capability of this method to detect the onset of damage and accurately quantify its progression. For low-velocity impacts, the damage indicator exhibits clear and consistent trends across different energy levels, correlating well with observations from X-ray tomography. Three distinct damage regimes were identified: negligible damage at low-impact energies, stable damage growth at moderate energies, and rapid damage accumulation at higher energies. These observations align with X-ray tomography imaging, which revealed progressive damage mechanisms such as matrix cracking, delamination, and fiber breakage, spreading through multiple composite layers as impact energy increased.

In fatigue loading scenarios, the GLW-based method demonstrated its robustness and reliability in detecting diffuse damage states and differentiating between undamaged and damaged samples. Despite more significant variability in fatigue damage due to the probabilistic nature of loading and the inherent heterogeneity of composite materials, the damage indicator correlated well with X-ray tomography results, including void volume ratio measurements. Notably, even unexpected trends in the fatigue data, such as a decrease in the void ratio for certain stress levels, were reflected in the proposed indicator, underscoring its robustness and reliability.

This work validates the proposed damage indicator through extensive experimental conditions, encompassing seven impact energy levels and nine fatigue loading configurations, ensuring its applicability to a wide range of practical scenarios. Furthermore, the methodology requires minimal sample preparation and provides a scalable, non-destructive solution for damage assessment. This makes it particularly suited for in-service monitoring of composite structures, offering a practical and efficient tool for industry.

This study advances the state of the art in non-destructive testing (NDT) for composite materials by offering a sensitive, practical, and scalable technique. The findings pave the way for applications in real-world composite structures, such as automotive body panels and aerospace components, where early damage detection is critical for ensuring safety and reliability.

Future work could extend this methodology to more complex loading configurations, such as fatigue post-impact or impact post-fatigue sequences, to better mimic real-world conditions. Applying this method to geometrically complex components would further validate its industrial relevance. Integrating guided Lamb wave analysis with computational tools like finite element modeling could also deepen understanding of wave-defect interactions in anisotropic and heterogeneous materials. The question of the influence of the temperature will need to be addressed for on-site inspection. Typically, temperature sensors are added to calibrate the measurement and limit the environment influence on it. This needs to be verified practically.

Further enhancement could also come from integrating machine learning algorithms to automate defect classification and severity prediction, enabling real-time damage assessment.

Acknowledgements The present work is supported by Groupe PSA and made in the framework of the Open-Lab Materials and Processes involving Groupe PSA, Arts et Metiers (ENSAM) and Georgia Tech Lorraine. The authors would like to thank DuPont de Nemours for their support and for providing the material of this study.

Author Contributions All authors contributed to the study conception and design. Material preparation, data collection and analysis were performed by Nada Miqoi and Pascal Pomarede. The first draft of the manuscript was written by Nada Miqoi and Pascal Pomarede and all authors commented on previous versions of the manuscript. All authors read and approved the final manuscript.

Funding Open access funding provided by Arts et Metiers Institute of Technology.

Data Availability No datasets were generated or analysed during the current study.

Declarations

Competing Interests The authors declare no competing interests.

References

1. Ishikawa, T., Amaoka, K., Masubuchi, Y., Yamamoto, T.: Overview of automotive structural composites technology developments in Japan. Compos. Sci. Technol. **155**, 221–246 (2018). https://doi.org/10.1016/j.compscitech.2017.09.015
2. Böhm, R., Hornig, A., Weber, T., Grüber, B., Gude, M.: Experimental and numerical impact analysis of automotive bumper brackets made of 2D triaxially braided CFRP composites. Mater. 2020. **13**(16), 3554 (Aug. 2020). https://doi.org/10.3390/MA13163554
3. Agrawal, S., Singh, K.K., Sarkar, P.-K.: Impact damage on fibre-reinforced polymer matrix composite – A review. J. Compos. Mater. **48**(3), 317–332 (2013). https://doi.org/10.1177/0021998312472217
4. Karayaka, M., Kurath, P.: Deformation and Failure Behavior of Woven Composite Laminates. Journal of Engineering Materials and Techology. **116**, no. April, 222–232 (1994)
5. Montesano, J., Fawaz, Z., Bougherara, H.: Non-destructive assessment of the fatigue strength and damage progression of satin woven fiber reinforced polymer matrix composites. Compos. Part. B: Eng. **71**, 122–130 (2015). https://doi.org/10.1016/j.compositesb.2014.11.005
6. Gul, S., Tabrizi, I.E., Okan, B.S., Kefal, A., Yildiz, M.: An experimental investigation on damage mechanisms of Thick hybrid composite structures under flexural loading using multi-instrument measurements. Aerosp. Sci. Technol. **117**, 106921 (2021). https://doi.org/10.1016/j.ast.2021.106921
7. Atas, C., Sayman, O.: An overall view on impact response of woven fabric composite plates. Compos. Struct. **82**, 336–345 (2008). https://doi.org/10.1016/j.compstruct.2007.01.014
8. Kara, M., Muhammed, K.: Effects of the number of fatigue cycles on the impact behavior of glass Fi Ber / epoxy composite tubes. Compos. Part. B: Eng. **123**, 55–63 (2017). https://doi.org/10.1016/j.compositesb.2017.04.021

9. Cui, J., Yan, S., Zhao, Y., Jiang, L.: Low-Velocity Impact and Residual Compression Performance of Carbon Fiber Reinforced Composite Stiffened Plates. Appl Compos Mater. **30**(4), 1185–1206, Aug. (2023). https://doi.org/10.1007/s10443-023-10121-z
10. Sadighi, M., Alderliesten, R.: Impact fatigue, multiple and repeated low-velocity impacts on FRP composites: A review. Compos. Struct. **297**, 115962 (Oct. 2022). https://doi.org/10.1016/J.COMPSTRUCT.2022.115962
11. Colombo, C., Bhujangrao, T., Libonati, F., Vergani, L.: Effect of delamination on the fatigue life of GFRP: A thermographic and numerical study. Compos. Struct. **218** (2019). https://doi.org/10.1016/j.compstruct.2019.03.023
12. Jollivet, T., Peyrac, C., Lefebvre, F.: Damage of composite materials. Procedia Eng. **66** (2013). https://doi.org/10.1016/j.proeng.2013.12.128
13. Osada, T., Nakai, A., Hamada, H.: Initial fracture behavior of satin woven fabric composites. Compos. Struct. **61**, 333–339 (2003). https://doi.org/10.1016/S0263-8223(03)00058-8
14. Budadin, O.N., Kozelskaya, S.O., Kaledin, V.O., Vavilov, V.P., Kuimova, M.V.: Evaluating impact damage to fabric-based personal armor by infrared NDT. Int. J. Damage Mech. (2019). https://doi.org/10.1177/1056789518823880
15. Katunin, A., Pivdiablyk, I., Gornet, L., Rozycki, P.: A hybrid method for determination of fatigue limit and non-destructive evaluation of composite structures after low-velocity impact loading. Compos. Part. B. **238**, 109898 (2022). https://doi.org/10.1016/j.compositesb.2022.109898
16. Evans, E.E., et al.: Feb., Comparison of X-ray Computed Tomography and Ultrasonic C-Scan Techniques and Numerical Modelling of Impact Damage in a CFRP Composite Laminate. Appl Compos Mater. **31**(1), 249–264 (2024). https://doi.org/10.1007/s10443-023-10171-3
17. Holmes, J., Sommacal, S., Stachurski, Z., Das, R., Compston, P.: Digital image and volume correlation with X-ray micro-computed tomography for deformation and damage characterisation of woven fibre-reinforced composites. Compos. Struct. **279**, 114775 (Jan. 2022). https://doi.org/10.1016/J.COMPSTRUCT.2021.114775
18. Srivastava, C., Agostino, P., Stamopoulos, A.G., Alcock, B., Strandlie, A., Grammatikos, S.: Three-Dimensional Analysis of Porosity in As-Manufactured Glass Fiber/Vinyl Ester Filament Winded Composites Using X-Ray Micro-Computed Tomography. Appl Compos Mater. **31**(1), 171–200 Feb. (2024). https://doi.org/10.1007/s10443-023-10167-z
19. Maier, A., Schmidt, R., Oswald-Tranta, B., Schledjewski, R.: Non-Destructive thermography analysis of impact damage on Large-Scale CFRP automotive parts. Materials. **7**, 413–429 (2014). https://doi.org/10.3390/ma7010413
20. Pastor, M.-L., Garnier, C., Pescay, C.: Comparison of two Non-destructive tests in carbon/epoxy composites. J. Mater. Sci. Eng., **4**, 10, (2010)
21. Aymerich, F., Meili, S.: Ultrasonic evaluation of matrix damage in impacted composite laminates. Compos. Part. B: Eng. **31**, 1–6 (2000)
22. Baste, S., Aristégui, C.: Induced anisotropy and crack systems orientations of a ceramic matrix composite under off-principal axis loading. Mech. Mater. **29**(1), 19–41 (1998). https://doi.org/10.1016/S0167-6636(98)00003-9
23. Marguères, P., Meraghni, F.: Damage induced anisotropy and stiffness reduction evaluation in composite materials using ultrasonic wave transmission. Compos. Part A: Appl. Sci. Manufac. **45**, 134–144 (2013)
24. Pomarède, P., Meraghni, F., Peltier, L., Delalande, S., Declercq, N.F.: Damage evaluation in woven glass reinforced polyamide 6. 6 / 6 composites using ultrasound Phase-Shift analysis and X-ray tomography. J. Nondestr. Eval. **37**(12) (2018). https://doi.org/10.1007/s10921-018-0467-3
25. Van Den Abeele, K.E., Johnson, P.A., Sutin, A.: Nonlinear elastic wave spectroscopy (NEWS) techniques to discern material damage, part I: Nonlinear wave modulation spectroscopy (NWMS). Res. Nondestr. Eval. **12**(1), 17–30 (2000). https://doi.org/10.1080/09349840009409646
26. Meo, M., Polimeno, U., Zumpano, G.: Detecting damage in composite material using nonlinear elastic wave spectroscopy methods. Appl. Compos. Mater. **15**, 115–126 (2008). https://doi.org/10.1007/s10443-008-9061-7
27. Eckel, S., Meraghni, F., Pomarède, P., Declercq, N.F.: Investigation of damage in composites using nondestructive nonlinear acoustic spectroscopy. Exp. Mech. **57**(2), 207–217 (2017). https://doi.org/10.1007/s11340-016-0222-6
28. Katunin, A., Wronkowicz-Katunin, A., Danek, W., Wyleżoł, M.: Modeling of a realistic barely visible impact damage in composite structures based on NDT techniques and numerical simulations. Compos. Struct. **267**, 113889 (Jul. 2021). https://doi.org/10.1016/j.compstruct.2021.113889
29. Smith, R.A.: Composite defects and their detection. in In: Materials Science and Engineering, vol. III, pp. 103–143. Encyclodpedia of Life Support Systems (2009)

30. Miqoi, N., et al.: Detection and evaluation of barely visible impact damage in woven glass fabric reinforced polyamide 6.6/6 composites using ultrasonic imaging, X-ray tomography and optical profilometry. Int. J. Damage Mech. **30**(3), 1–26 (2020). https://doi.org/10.1177/1056789520957703
31. Cawley, P., Alleyne, D.N.: The use of lamb waves for the long range inspection of large structures. Ultrasonics. **34**(2), 287–290 (1996). https://doi.org/10.1016/0041-624X(96)00024-8
32. Ouabi, O.-L., Pomarède, P., Declercq, N.F., Zeghidour, N., Geist, M., Pradalier, C.: Learning the propagation properties of rectangular metal plates for lamb wave-based mapping. Ultrasonics. **123**, 106705 (Feb. 2022). https://doi.org/10.1016/J.ULTRAS.2022.106705
33. Luo, K., Liu, Y., Liang, W., Chen, L., Yang, Z.: Rapid damage reconstruction imaging of composite plates using non-contact air-coupled lamb waves. NDT E Int. 103047 (Jan. 2024). https://doi.org/10.1016/j.ndteint.2024.103047
34. Castaings, M., Singh, D., Viot, P.: Sizing of impact damages in composite materials using ultrasonic guided waves. NDT E Int. **46**, 22–31 (2012). https://doi.org/10.1016/j.ndteint.2011.10.002
35. Chehami, L., Moulin, E., Rosny, J.D., Prada, C., Matar, O.B., Benmeddour, F.: Detection and localization of a defect in a reverberant plate using acoustic field correlation. J. Appl. Phys. **115** (2014). https://doi.org/10.1063/1.4867522
36. Jingpin, J., Xiangji, M., Cunfu, H., Bin, W.: Nonlinear lamb wave-mixing technique for micro-crack detection in plates. NDT E Int. **85**, 63–71 (2017). https://doi.org/10.1016/j.ndteint.2016.10.006
37. Zheng, K., Li, Z., Ma, Z., Chen, J., Zhou, J., Su, X.: Damage detection method based on lamb waves for stiffened composite panels. Compos. Struct. **225**, 111137 (Oct. 2019). https://doi.org/10.1016/J.COMPSTRUCT.2019.111137
38. He, C., Liu, H., Liu, Z., Wu, B.: The propagation of coupled Lamb waves in multilayered arbitrary anisotropic composite laminates. Journal of Sound and Vibration. **332**(26), 7243–7256, Dec. (2013). https://doi.org/10.1016/J.JSV.2013.08.035
39. Azuara, G., Barrera, E., Ruiz, M., Bekas, D.: Damage Detection and Characterization in Composites Using a Geometric Modification of the RAPID Algorithm. IEEE Sensors J. **20**(4), 2084–2093, Feb. (2020). https://doi.org/10.1109/JSEN.2019.2950748
40. Mustapha, S., Ye, L., Dong, X., Alamdari, M.M.: Evaluation of barely visible indentation damage (BVID) in CF/EP sandwich composites using guided wave signals. Mech. Syst. Signal Process. 76–77 (Aug. 2016). https://doi.org/10.1016/j.ymssp.2016.01.023
41. He, J., Yuan, F.-G., RD Annual Review of Progress in Quantitative Nondestructive Evaluation: Lamb wave-based BVID imaging for a curved composite sandwich panel, presented at the 43, VOLUME 36, Atlanta, Georgia, USA, p. 050012. (2017). https://doi.org/10.1063/1.4974606
42. Li, Z., et al.: Baseline-free assisted lamb wave-based damage detection in CFRP composites using graph convolutional networks and transformer models. Measurement. **242**, 116159 (Jan. 2025). https://doi.org/10.1016/j.measurement.2024.116159
43. Malpot, A., Touchard, F., Bergamo, S.: Etude du comportement en fatigue d ' un composite à matrice thermoplastique tissé de fibres de verre pour application automobile Study of the behaviour of a woven glass-fibre-reinforced composite with a thermoplastic matrix for automotive application, in Journées Nationales des Compositees 19, Lyon, pp. 1–9. (2015)
44. Basquin O.H.: The exponential law of endurance tests. Am. Soc. Test. Mater. Proc. **10**, 625–630 (1910)
45. Lomov, S.V., et al.: Predictive analyses and experimental validations of effective elastic properties of 2D and 3D woven composites, in 13th European Conference on Composite Materials (ECCM-13), Stockholm, (2008)
46. Praud, F.: Multi-scale modelling of thermoplastic-based woven composites, cyclic and time-dependent behaviour, Ecole Nationale Supérieure d'Arts et Métiers, 2018. [Online]. Available: https://pastel.archives-ouvertes.fr/tel-01936624/document
47. Praud, F., Chatzigeorgiou, G., Meraghni, F.: Fully integrated multi-scale modelling of damage and time-dependency in thermoplastic-based woven composites: International Journal of Damage Mechanics. **30**(2), 163–195, Sep. (2020). https://doi.org/10.1177/1056789520944986
48. Ochôa, P., Infante, V., Silva, J.M., Groves, R.M.: Detection of multiple low-energy impact damage in composite plates using Lamb wave techniques. Composites Part B: Engineering. **80**, 291–298, Oct. (2015). https://doi.org/10.1016/j.compositesb.2015.06.010
49. Su, Z., Ye, L., Lu, Y.: Guided lamb waves for identification of damage in composite structures: A review. J. Sound Vib. **295**, 753–780 (2006). https://doi.org/10.1016/j.jsv.2006.01.020
50. Babout, L., Maire, E., Buffière, J.Y., Fougères, R.: Characterization by x-ray computed tomography of decohesion, porosity growth and coalescence. Acta Mater. **49**, 2055–2063 (2001)
51. Mehdikhani, M., Gorbatikh, L., Verpoest, I., Lomov, S.V.: Voids in fiber-reinforced polymer composites: A review on their formation, characteristics, and effects on mechanical performance. J. Compos. Mater. **53**(12), 1579–1669 (2019). https://doi.org/10.1177/0021998318772152

Authors and Affiliations

Nada Miqoi[1,2,3] · Pascal Pomarède[1] · Fodil Meraghni[1] · Nico Félicien Declercq[2] · Stéphane Delalande[4]

✉ Pascal Pomarède
pascal.pomarede@ensam.eu

Nada Miqoi
nada.miqoi@ensam.eu

Fodil Meraghni
fodil.meraghni@ensam.eu

Nico Félicien Declercq
declercq@gatech.edu

Stéphane Delalande
stephane.delalande2@lecnam.net

[1] Arts et Métiers Institute of Technology, CNRS, LEM3-UMR CNRS 7239, 4 rue Augustin Fresnel, Metz 57078, France

[2] George W. Woodruff School of Mechanical Engineering, Georgia Institute of Technology, Atlanta, GA, USA; GeorgiaTech Europe, IRL 2958 Georgia Tech – CNRS, 2 rue Marconi, Metz 57070, France

[3] Stellantis – Centre technique de Vélizy, Route de Gisy, Vélizy-Villacoublay 78140, France

[4] CNAM, CNRS, PIMM UMR8006, 292 rue Saint Martin, Paris 75003, France